THE JOURNAL OF COMPARATIVE NEUROLOGY 366:416–430 (1996)

Heterogeneous Axonal Arborizations of Rat Thalamic Reticular Neurons in the Ventrobasal Nucleus

CHARLES L. COX, JOHN R. HUGUENARD, AND DAVID A. PRINCE
Department of Neurology and Neurological Sciences, Stanford University Medical Center, Stanford, California 94305

ABSTRACT

The γ-aminobutyric acid (GABA)-containing neurons of the thalamic reticular nucleus (nRt) are a major source of inhibitory innervation in dorsal thalamic nuclei. Individual nRt neurons were intracellularly recorded and labelled in an in vitro rat thalamic slice preparation to investigate their projection into ventrobasal thalamic nuclei (VB). Camera lucida reconstructions of 37 neurons indicated that nRt innervation ranges from a compact, focal projection to a widespread, diffuse projection encompassing large areas of VB. The main axons of 65% of the cells gave rise to intra-nRt collaterals prior to leaving the nucleus and, once within VB, ramified into one of three branching patterns: cluster, intermediate, and diffuse. The cluster arborization encompassed a focal region averaging approximately 25,000 μm^2 and contained a high density of axonal swellings, indicative of a topographic projection. The intermediate structure extended across an area approximately fourfold greater and also contained numerous axonal swellings. The diffuse arborization of nRt neurons covered a large region of VB and contained a relatively low density of axonal swellings. Analysis of somatic size and shape revealed that diffuse arborizations arose from significantly smaller, fusiform-shaped somata. Cytochrome oxidase reactivity or parvalbumin immunoreactivity was used to delineate a discontinuous staining pattern representing thalamic barreloids. The size of a cluster arborization closely approximated that of an individual barreloid. The heterogeneous arborizations from nRt neurons may reflect a dynamic range of inhibitory influences of nRt on dorsal thalamic activity.

Indexing terms: thalamic inhibition, somatosensory system, thalamus, nucleus reticularis, anatomy

The thalamic reticular nucleus (nRt) is composed of a thin layer of γ-aminobutyric acid (GABA)-containing neurons and encompasses the anterior, lateral, and ventral extent of the dorsal thalamus (Jones, 1985). Virtually all thalamocortical (TC) and corticothalamic (CT) fibers pass through nRt. Collaterals from these traversing fibers serve as the primary synaptic input for nRt neurons (Ohara and Lieberman, 1981; Jones, 1985), whereas the major output of nRt is to underlying dorsal thalamic nuclei (Scheibel and Scheibel, 1966; Minderhoud, 1971; Jones, 1975). Consequently, excitation of nRt neurons by CT fibers provides feedforward inhibition of neurons in relay nuclei, whereas excitatory input from TC axons evokes feedback inhibition onto TC neurons. Functionally, this intimate relationship between nRt and dorsal thalamus can modify the flow of information from thalamus to cortex and can play a role in shaping receptive fields of dorsal thalamic neurons (Yingling and Skinner, 1976; Hale et al., 1982; Ahlsén et al., 1985; Shosaku et al., 1989; Lee et al., 1994). In addition, the reciprocal synaptic connectivity between nRt and dorsal thalamic nuclei can generate oscillatory neuronal rhythms (Steriade et al., 1993; von Krosigk et al., 1993; Huguenard and Prince, 1994b), whose occurrence has been associated with periods of decreased arousal and pathophysiological conditions, such as generalized absence epilepsy (Williams, 1953; Domich et al., 1986; Steriade and Llinás, 1988).

Clearly, the primary output of nRt is in dorsal thalamus; however, the topographical extent of this innervation is uncertain. Studies using extracellular tracer injections have demonstrated both a focal as well as a nonspecific diffuse relationship between nRt and dorsal thalamus (Jones, 1975; Montero et al., 1977; Crabtree and Killackey, 1989; Conley and Diamond, 1990; Crabtree, 1992; Liu et al., 1995). Few studies have examined directly the efferents of individual nRt neurons in dorsal thalamus to

Accepted September 28, 1995.

Address reprint requests to Charles L. Cox, Ph.D. Department of Neurology and Neurological Sciences, Room M016, Stanford University School of Medicine, Stanford, CA 94305.

resolve this inconsistency. Early Golgi studies revealed that axonal projections from individual nRt neurons give rise to a divergent axonal arborization that encompasses a relatively broad area of the target thalamic relay nucleus (Scheibel and Scheibel, 1966). Intracellular labelling of individual nRt neurons with horseradish peroxidase (HRP) clearly defined a diffuse axonal projection of individual nRt neurons in ventrobasal thalamic nuclei (VB) and also demonstrated that a single nRt neuron can innervate multiple thalamic nuclei (Yen et al., 1985). These results suggest that nRt-thalamic projections lack the precise topographical organization characteristic of thalamocortical and corticothalamic projections. In contrast to these findings, intracellular injections of single cells within the perigeniculate nucleus, which is a structure analogous to nRt in the visual dorsal thalamus, reveal that individual neurons have both a focal and a diffuse axonal arborization (Uhlrich et al., 1991). Furthermore, extracellular labelling of single nRt neurons indicates a focal axonal projection within somatosensory dorsal thalamus (Pinault et al., 1995a).

The influence of nRt on thalamocortical function will be affected significantly by the spatial extent of axonal projections from individual nRt neurons in the dorsal thalamus. Because virtually all of its cells are GABA containing (Houser et al., 1980), nRt serves as a major inhibitory influence on thalamocortical neurons. Furthermore, because rodent dorsal thalamus, with the exception of the lateral geniculate nucleus (LGN; Ottersen and Storm-Mathisen, 1984), lacks inhibitory interneurons, nRt functions as its primary source of inhibition. Divergent nRt projections would support a widespread inhibitory influence of nRt in dorsal thalamus. However, certain activities that rely on the reciprocal connectivity of nRt and dorsal thalamus, such as intrathalamic rhythmic oscillations and focal receptive fields, may require a more restricted topographic relationship.

In these experiments, we have examined the morphology of axonal arborizations originating from individual nRt neurons that project to VB. Tight-seal, whole-cell, patch-clamp recordings were obtained simultaneously to investigate intrinsic neuronal properties and to label individual nRt neurons. Our findings indicate that individual nRt neurons give rise to a heterogeneous population of axonal arborizations, ranging from a very restricted focal projection to a widespread, divergent one. The focal axonal arborizations could serve as an anatomical correlate for a precise topographical relationship between nRt and dorsal thalamus. Although the axonal arborizations of individual nRt neurons can vary significantly, the intrinsic properties of these cells are quite similar. Some of these findings have appeared in abstract form (Cox et al., 1994).

MATERIALS AND METHODS

Young Sprague-Dawley rats (postnatal age, 10–16 days) were deeply anaesthetized with sodium pentobarbital (55 mg/kg) and decapitated, and the brains were quickly removed and placed into chilled oxygenated slicing medium (4°C). Thalamic slices (400–450 μm) were cut in the horizontal plane (Huguenard and Prince, 1994a) by using a Vibratome (TPI, St. Louis, MO) and were transferred to a holding chamber containing oxygenated physiological saline (31°C) for at least 2 hours prior to recording. The slicing medium contained (in mM) 2.5 KCl, 1.25 NaH_2PO_4, 10.0 $MgCl_2$, 0.5 $CaCl_2$, 26.0 $NaHCO_3$, 11.0 glucose, and 234.0 sucrose. The physiological saline contained (in mM) 126.0 NaCl, 2.5 KCl, 1.25 NaH_2PO_4, 2.0 $MgCl_2$, 2.0 $CaCl_2$, 26.0 $NaHCO_3$, and 10.0 glucose. Both solutions had a pH of 7.4 when gassed with 95% O_2 and 5% CO_2. Following incubation, the slices were transferred to a recording chamber maintained at 35 ± 1°C and were superfused with physiological saline at a rate of 1.3 ml/minute.

Whole-cell recordings were made by using the "blind" patch technique (Blanton et al., 1989). Recording pipettes were pulled from borosilicate capillary glass (1.5 mm O.D.; Garner Glass Company) by using a two-stage vertical pipette puller (PP-83; Narishige). The pipettes had a tip resistance of 4 to 6 MΩ when they were filled with the following solution (in mM): 117 K-gluconate, 13 KCl, 1.0 $MgCl_2$, 0.07 $CaCl_2$, 0.1 ethylene glycol-O,O′-bis(2-aminoethyl)-N,N,N′,N′-tetraacetic acid (EGTA), 10.0 N-(2-hydroxyethyl)piperazine-N′-(2-ethanesulfonic acid; HEPES), 2.0 Na_2-ATP, 0.4 Na-GTP, and biocytin (0.5%), pH 7.3. Following formation of a high-resistance seal (1–4 GΩ), a brief negative-pressure pulse was applied to the recording pipette, and a whole-cell recording configuration was obtained with an initial access resistance ranging from 15 to 50 MΩ.

Current clamp recordings were obtained by using an Axoclamp 2A amplifier (Axon Instruments) in the bridge mode. Data were collected on line using computer-based data acquisition software (Pclamp; Axon Instruments) and were recorded on a chart recorder and on magnetic tape (Neurodata) for later analysis. The apparent input resistance (R_N) was determined from the linear slope of the voltage/current relationship obtained by applying constant current pulses ranging from −110 to 40 pA. Membrane time constant (τ_m) was estimated by fitting a single exponential decay function to the membrane response evoked by a small hyperpolarizing current pulse (20 or 50 pA).

Following the recordings, slices were fixed in either 4% paraformaldehyde or 4% paraformaldehyde/0.3% glutaraldehyde in 0.1 M phosphate buffered saline (PBS) overnight. The procedures that were used for processing the biocytin-filled neurons were similar to those previously described (Horikawa and Armstrong, 1988; Tseng et al., 1991). Briefly, following fixation, the slices were resectioned at 80 μm, treated with 0.25% Triton X-100 and 2% bovine serum albumin in 0.1 M PBS, and then incubated in an avidin-biotin-HRP complex (ABC kit PK-4000; Vector Laboratories). Following the diaminobenzidine reaction, osmium tetroxide (1.0%) in Tris buffer (0.1 M) was used to intensify the reaction product. The sections were then mounted, air dried, and counterstained with cresyl violet to identify the boundaries of VB and nRt. All compounds used were purchased from Sigma, unless otherwise noted.

For histochemical experiments, male Sprague-Dawley rats (postnatal age, 10–13 days; n = 7) were anesthetized as before and were transcardially perfused with saline followed by 4% paraformaldehyde in 0.1 M PBS. The brains were removed and postfixed in the paraformaldehyde solution for an additional 2–24 hours. The tissue was then sectioned at 50 μm using a Vibratome or a freezing-stage microtome. When using the latter method, the tissue was cryoprotected with 25% sucrose-containing PBS prior to sectioning. The procedures used for cytochrome-oxidase staining were similar to those described by Wong-Riley (1979). For the immunohistochemistry, antiparvalbumin

(anti-PV) antibody was obtained from Sigma. The sections were washed in 0.1 M PBS and were then incubated with the anti-PV (1:1,000), 10% normal horse serum, and 0.3% Triton X-100 for 17 hours. The sections were then incubated in the secondary antibody, anti-mouse immunoglobulin (IgG; 1:100) in 0.1 M PBS, and were tagged with either HRP or Texas red.

Camera lucida reconstructions were made of all labelled neurons and their axonal arborizations using a Leitz Dialux 20 microscope and either ×16 or ×25 objectives. Somata were reconstructed using a water-immersion, Hoffman-modified ×50 objective. For nRt neurons that were included in the analysis of bouton size and density, reconstructions were made using the ×50 water-immersion or the ×100 oil-immersion objective. Drawings were then further enlarged on a photocopier (156% for ×100 drawings; 243% for ×50 drawings) to improve the reliability of the measurements. The lengths and areas of somata and axonal arborizations and perimeters of axonal swellings (boutons) were measured by using Sigmascan digitization software (Jandel Scientific). The areas of dendritic arborizations of VB neurons were also measured from these drawings. In three neurons, bouton perimeters were measured twice to verify the consistency of the observations. Bouton densities were determined by counting the number of boutons in a series of 30 × 30 μm grids extending across the entire arborization. Statistical analyses consisted primarily of either Student's t test or an analysis of variance. Differences between the distributions of bouton perimeters were tested by using the Kolmogorov-Smirnov test (K-S test; Press et al., 1986) and were considered significant when $P < 0.05$. All averages are presented as mean ± standard error of the mean, unless otherwise noted.

RESULTS

Axonal arborizations of nRt neurons

Thirty-seven intracellularly labelled nRt neurons with extensive axonal arborizations in VB were included in the present study. These neurons had stable resting potentials and overshooting action potentials indicative of satisfactory somatic recordings. The somata and dendrites of the labelled neurons were completely contained within the boundaries of nRt. The main axon of the nRt neuron originated normally from either the soma or a proximal dendrite. Sixteen of twenty-five neurons in which the main axon was clearly distinguishable within the dendritic field gave rise to intra-nRt collaterals that were typically short (< 100 μm) with few branches and never projected beyond the lateral extent of the dendrites (see Fig. 5Dii). The occurrence of these collaterals was not associated with any one of the particular types of axonal arborization described below. The main axon then projected toward VB either as a single axon (see, e.g., Figs. 1A, 3) or after dividing into multiple branches (see, e.g., Figs. 1B, 2). When the axon approached its target in VB, it ramified into one of three different arborization patterns, which we will term cluster, intermediate, and diffuse. Although the ventrobasal complex consists of two primary subdivisions, the ventroposteromedial (VPM) and the ventroposterolateral (VPL) nuclei (for review, see Jones, 1985), the different arborization patterns were observed throughout VB and did not appear to be restricted to either one of these specific subdivisions.

Cluster axonal arborizations

A striking characteristic of the cluster arborization is the restricted area that this structure encompasses. Representative cluster arborizations are illustrated in Figure 1. This compact structure could arise from either a single- (Fig. 1A) or a multiple-branched main axon (Fig. 1B). Closer examination of the cluster arborization revealed that it had a large number of short axonal branches originating from the main axon (Fig. 4A). These branches contained numerous swellings (Fig. 4Aii), giving this axonal structure an overall appearance similar to clusters of grapes. When viewed in two dimensions in the horizontal plane, the cluster structure encompassed an average area of 24,181 ± 2,873 μm^2 (n = 11; range, 14,312–44,104 μm^2), with a major axis (length) of 298 ± 38 μm (range, 145–479 μm) and width (perpendicular to that axis) of 120 ± 11 μm (range, 77–172 μm). The restricted size of the cluster arborization provides direct evidence for a focal projection of nRt neurons in dorsal thalamus.

Next, we compared the sizes of the cluster arborizations to the area of the dendritic fields of VB neurons. The average two-dimensional dendritic field of 11 reconstructed VB neurons in horizontal sections was 47,139 ± 6,820 μm^2 (range, 23,889–58,870 μm^2). Thus, the average area of the cluster arborization (24,181 μm^2) is approximately 50% of the dendritic area of a VB neuron, suggesting that the cluster may be in contact with a relatively small number of VB relay cells.

Intermediate axonal arborizations

At first glance, the intermediate arborization was similar in appearance to the cluster. At its target in VB, the main axon gave rise to a branching structure (Fig. 2) that had an average length of 583 ± 55 μm (range, 355–953 μm) and width of 359 ± 52 μm (range, 160–716 μm), dimensions that were significantly greater than those of the cluster arborization ($P < 0.01$). These intermediate axonal arbors encompassed an average area of 116,540 ± 15,067 μm^2 (n = 11; range, 65,626–247,267 μm^2), or about fourfold larger than that of the cluster arborization. Closer examination revealed that the intermediate arborization also had a complex axonal branching pattern; however, the collaterals off the main axon as well as the subsequent branches appeared to be longer and less dense than those of the cluster (Fig. 4Bi,ii). A relatively large number of axonal swellings were present within the intermediate arborization (Fig. 4Bii).

Diffuse axonal arborizations

The diffuse axonal arborization resembled the ramification pattern that has been described previously (Scheibel and Scheibel, 1966; Yen et al., 1985). The main axon gave rise to multiple branches in VB, and each of these branches ramified divergently (Fig. 3). An obvious difference between the diffuse structure and the other two axon types was the decreased complexity of axonal branching in the former. Although the axonal branching pattern of the intermediate and diffuse arborizations appeared to be somewhat similar in the collapsed two-dimensional camera lucida reconstructions (c.f. Figs. 2, 3), in a given microscopic field, these two populations were easily distinguishable. Comparable photo-

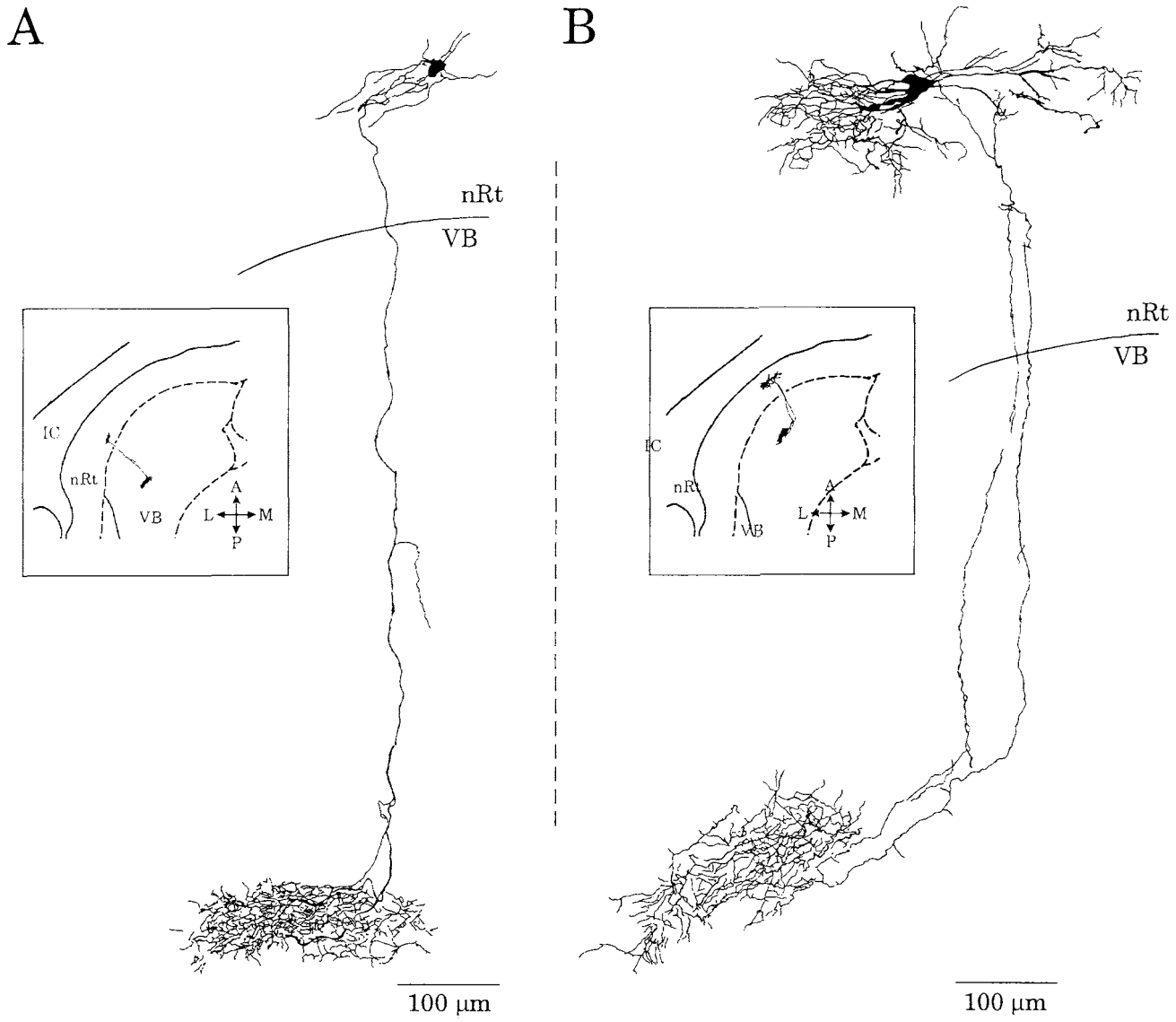

Fig. 1. **A,B:** Camera lucida reconstructions of two thalamic reticular nucleus (nRt) neurons with cluster axonal arborizations in VB. Note the extensive branching within a localized area. The **inset** is a schematic of the horizontal section modified from Paxinos and Watson (1986), indicating the location and orientation of the neuron within the slice. Similar insets are used in Figures 2 and 3. Drawings here and in Figures 2 and 3 were made from horizontal slices. A, anterior; L, lateral; M, medial; P, posterior; IC, internal capsule; nRt, nucleus reticularis thalami; VB, ventrobasal nuclear complex.

micrographs of relatively dense branching regions for each axonal arborization type are shown in Figure 4. Both the cluster structure and the intermediate structure contained many branches at a given focal depth (Fig. 4Ai,Bi); however, very few branches were present in the diffuse structure (Fig. 4Ci). The cluster and intermediate structures typically had relatively short interbranch lengths (Fig. 4A,B), whereas axonal branches in the diffuse arborizations tended to be longer (Fig. 4C). In the majority of neurons, the area of diffuse arborizations could not be quantified, because, unlike the cluster or intermediate arborizations, the structure was not completely contained within a single 400–450-μm-thick slice. A second obvious difference between the diffuse arborizations and the other arborization types was the density of the axonal swellings or putative boutons. The cluster arborization contained an abundance of axonal swellings (Fig. 4Aii), whereas both the intermediate (Fig. 4Bii) and the diffuse structures (Fig. 4Cii) had far fewer axonal swellings.

Soma types

Because some studies have suggested that nRt neurons are a heterogeneous population distinguishable by somatic and dendritic characteristics (Spreafico et al., 1988, 1991), we examined filled cells to determine whether different axonal arborizations were associated with different types of somata. In general, the soma shapes could be divided into two primary types: fusiform and round (Fig. 5). Typically, the major axis of the fusiform-shaped somata was oriented parallel to the border of nRt and VB, and the primary dendrites emerged from the poles of the soma, extending in

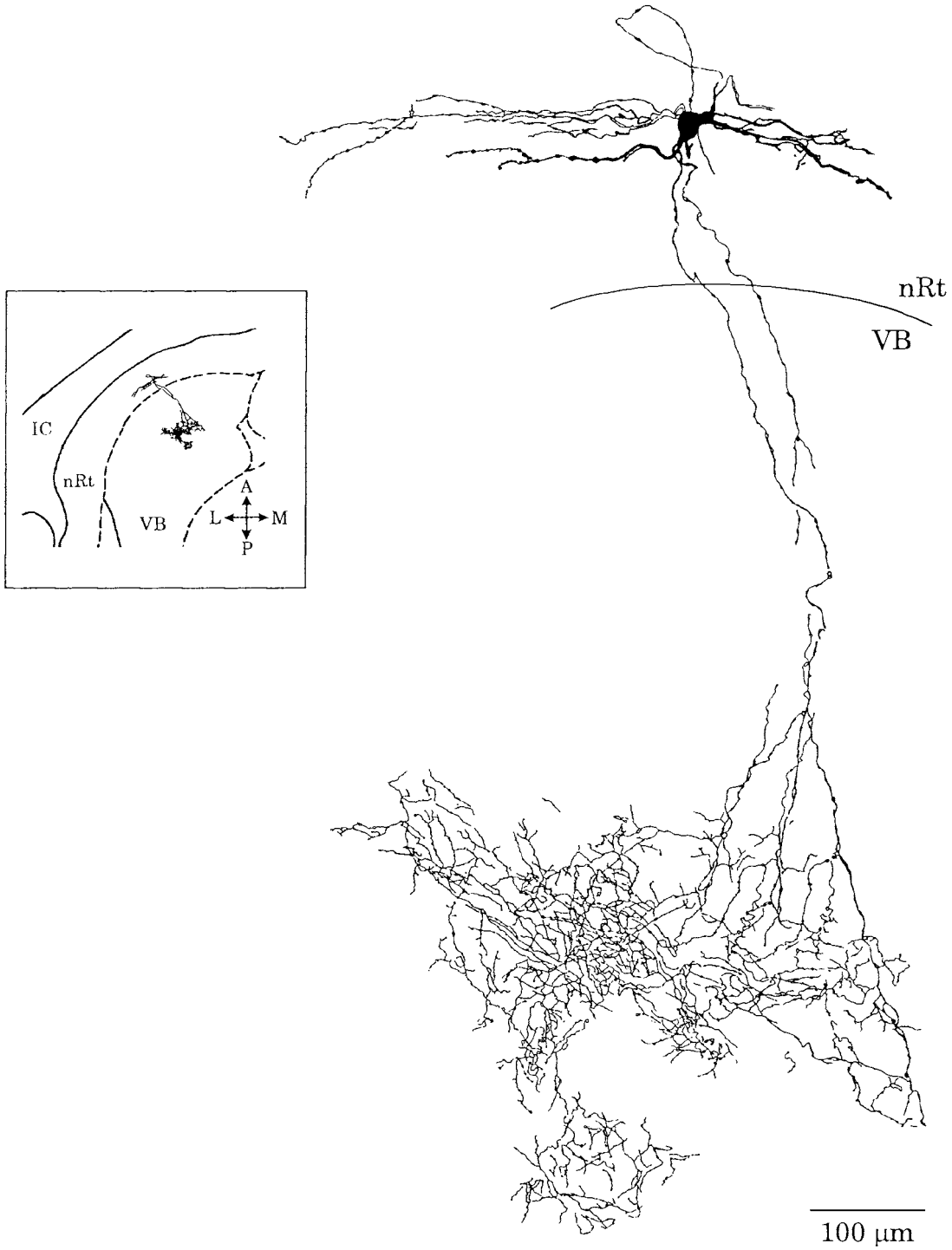

Fig. 2. Camera lucida reconstruction of an nRt neuron with an intermediate type of axonal arborization. Note the extensive arborization of the axon. For abbreviations, see Figure 1.

the same plane as the soma (Fig. 5A,B). The primary dendrites gave rise to multiple secondary dendrites that branched farther, usually ending with distal axon-like dendrites (see, e.g., Fig. 5Cii, arrows). The primary dendrites of round somata could emerge from any side of the soma (Fig. 5Ci,Di) and were similar to those of the fusiform-shaped cells, in that the dendrites had multiple branches that typically ended in axon-like appendages (Fig. 5Cii). The intermediate or cluster axonal arborizations were each associated with fusiform-shaped somata in approximately

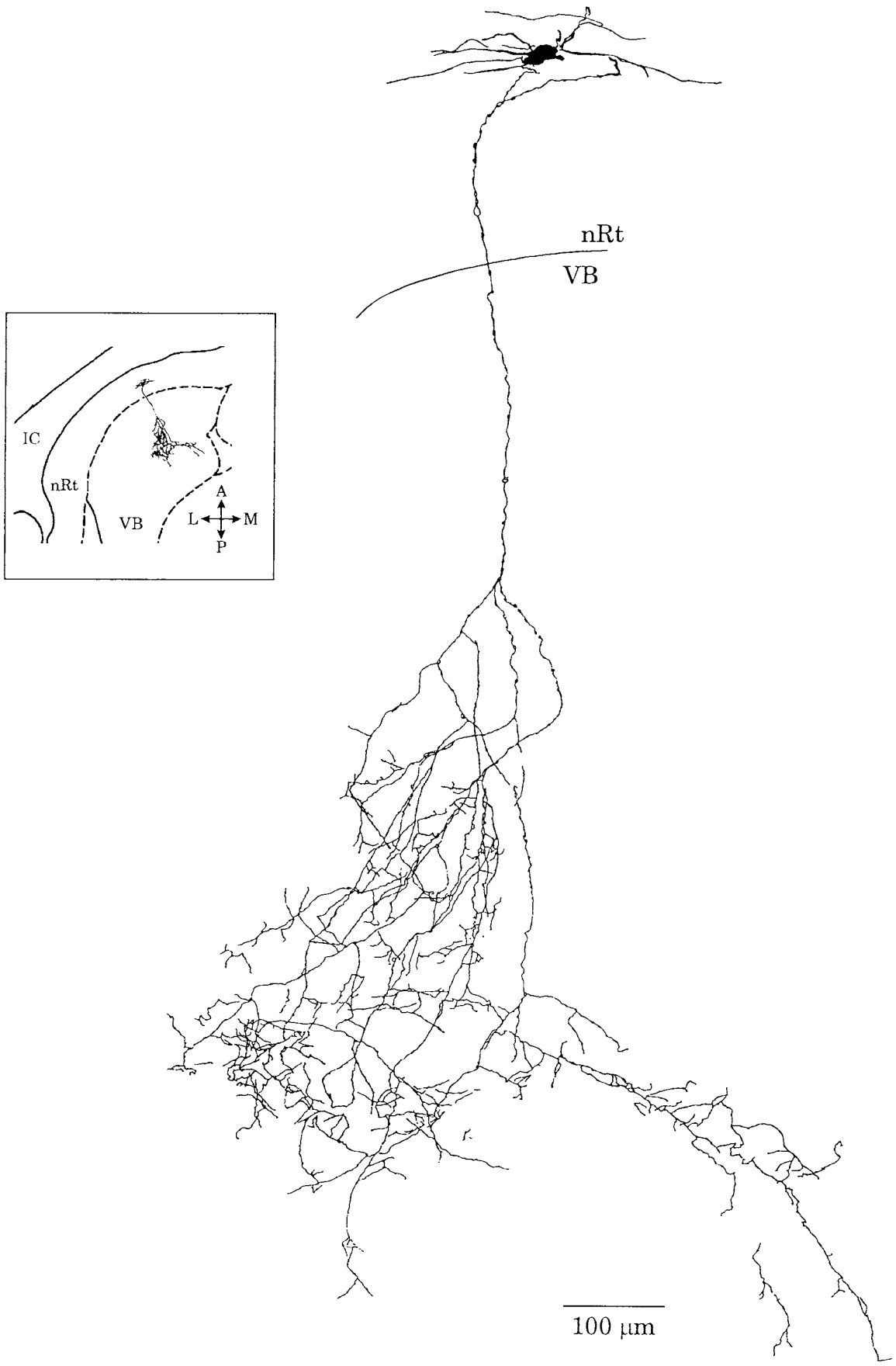

Fig. 3. Reconstruction of an nRt neuron with a diffuse type of axonal arborization. For abbreviations, see Figure 1.

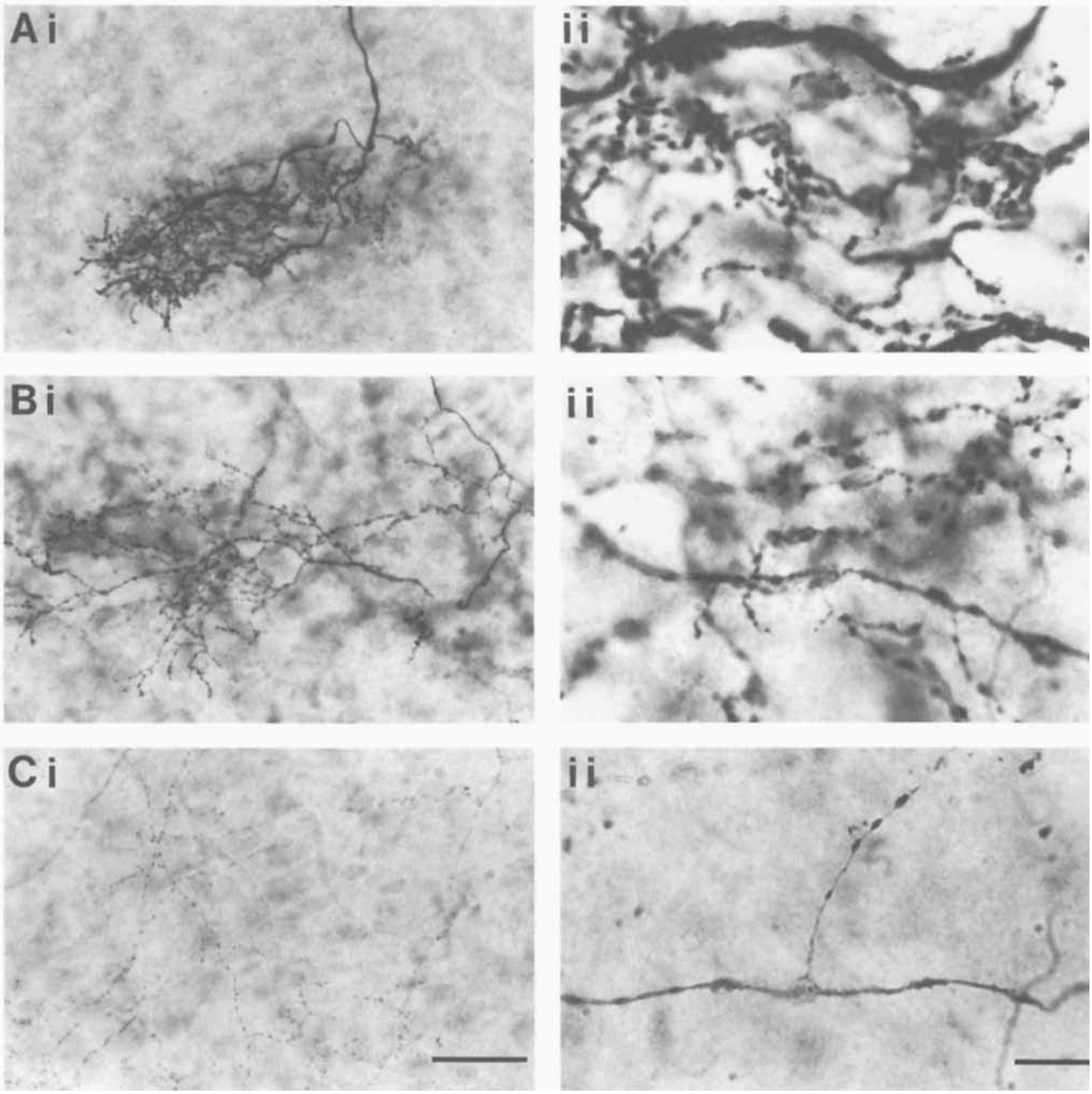

Fig. 4. Photomicrographs of single 80 μm sections containing different axonal arborizations. **Ai:** The same cluster arborization that is shown in Figure 1A. Note the compact size of the structure and the extensive and complicated branching pattern of the axon. **Aii:** At higher magnification, the axonal swellings are obvious. At a given focal plane, there are numerous swellings detected, suggesting a relatively high density of swellings in this structure. **Bi,ii:** Photomicrographs of the intermediate arborization illustrated in Figure 2. Magnifications are the same as in Ai and Aii, respectively. In this structure, there is a decrease in the number of branches as well as a decrease in the axonal swellings compared to the cluster specialization in a given plane of section. **Ci,ii:** Comparable magnifications of the diffuse arborization. These micrographs were taken at a region of relatively high density. Note that only a few axon branches are present in the same focal plane compared to the intermediate and the cluster. At higher magnification (Cii), there is an obvious decrease in the density of axonal swellings. Scale bars = 50 μm in Ci (also applies to Ai,Bi), 10 μm in Cii (also applies to Aii,Bii).

60% of neurons and with round somata in the remainder. By contrast, 12 of 14 diffuse arborizations (85%) were associated with fusiform somata.

Variations in somatic size were observed among nRt cells with different axonal arborizations (Table 1). Although there was no significant difference in the somatic areas of neurons with cluster (467.9 ± 34.1 μm^2) vs. intermediate arborizations (509.9 ± 50.1 μm^2; $P > 0.1$), somata of cells with diffuse arborizations were significantly smaller than either of the other types (343.9 ± 25.1 μm^2; $P < 0.05$). Whereas somatic lengths (major axis) were not significantly different between neurons with the three types of axonal arbors ($P > 0.1$), the width (minor axis) of neurons associated with diffuse arborizations was significantly less than that of cells with cluster- or intermediate-type arbors ($P < 0.05$).

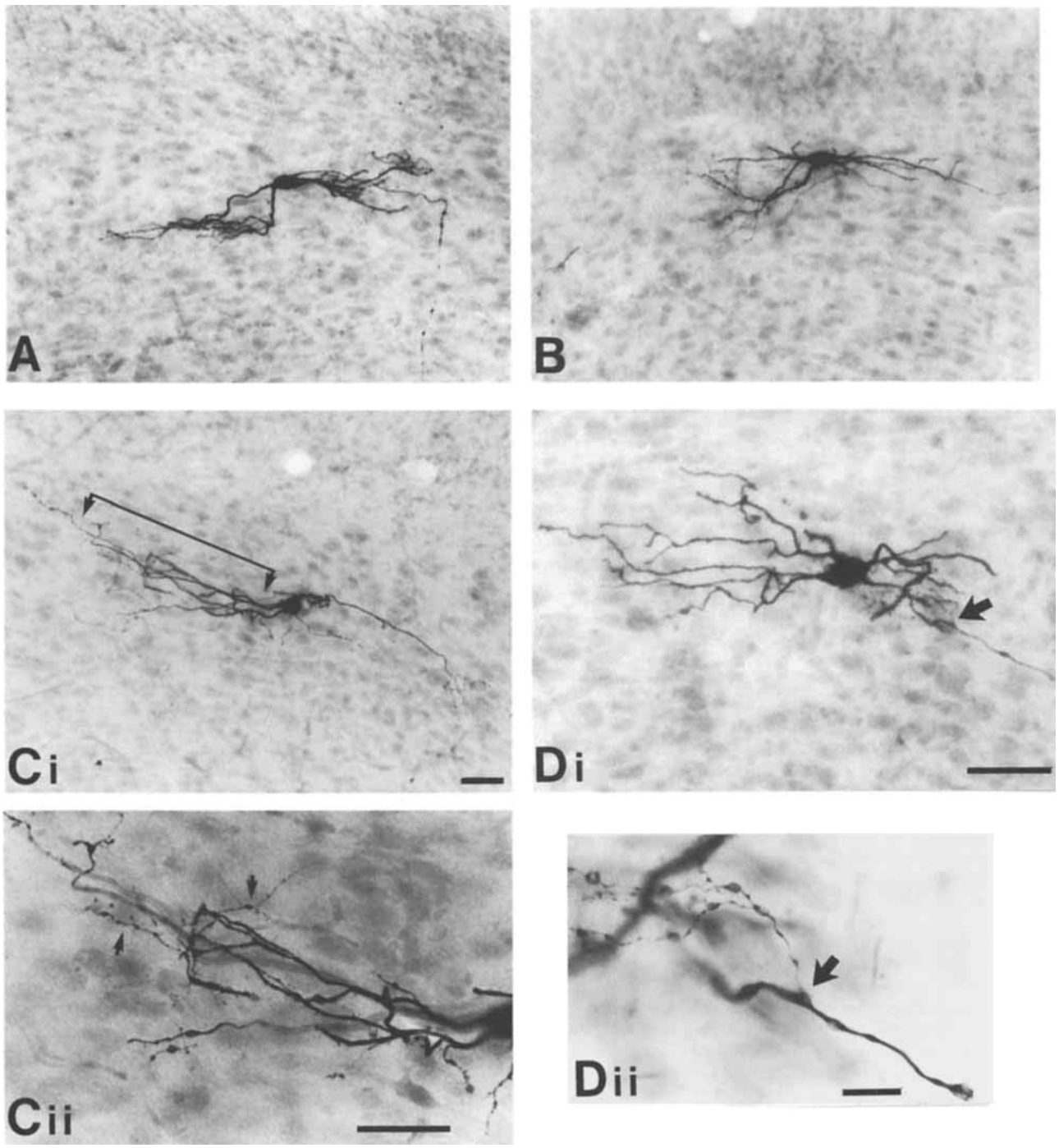

Fig. 5. Photomicrographs of biocytin-filled nRt neurons. **A,B:** Fusiform-shaped somata with primary dendrites emerging from the poles of the soma. The distal portion of the dendrites appear beaded and axon-like. **Ci,Di:** Round-shaped somata with primary dendrites emerging perpendicular to the longitudinal axis of the soma. **Cii:** Higher magnification of the dendrites shown between the arrows in Ci. Arrowheads point to fine, beaded, axon-like dendrites that extend from the thicker dendrites of the nRt neurons. Di: The axon of this neuron appears to branch within nRt (arrow), presumably giving rise to intra-nRt synaptic innervation. **Dii:** Higher magnification indicates that the fine collateral (arrow) gives rise to mutlibranching, beaded, axonal fibers. Scale bars = 50 μm in Ci (also applies to A,B,Ci), 50 μm in Cii (also applies to Di), 10 μm in Dii.

Axonal swellings

Under higher magnification, axonal swellings (boutons) were apparent in each type of arborization (Fig. 4Aii, Bii,Cii). Bouton size and density were quantified and compared in 11 neurons (four clusters, four intermediate, and three diffuse). Bouton perimeters in the cluster arborization were the smallest (3.5 ± 1.5 μm; mean ± S.D.; n = 2,968); whereas those in the diffuse (4.3 ± 1.8 μm; n = 1,394) and intermediate (4.5 ± 1.7 μm; n = 6,400) arborizations were larger and were similar to one another in size.

TABLE 1. Somatic Characteristics Associated With Different Axonal Arborizations

Arborization	Area (μm^2)	Length (μm)	Width (μm)
Cluster (n = 9)	467.9 ± 34.1 (320–579)	32.0 ± 3.3 (20.5–45.3)	19.0 ± 1.0 (15.4–23.7)
Intermediate (n = 9)	509.9 ± 50.1 (380–817)	31.8 ± 1.7 (23.2–39.3)	20.2 ± 1.6 (15.0–26.6)
Diffuse (n = 11)	343.9 ± 25.1 (206–472)*	30.8 ± 1.7 (23.5–40.4)	15.0 ± 0.9 (10.4–19.2)*

*$P < 0.01$ and 0.05 between diffuse and both intermediate and cluster, respectively (one-way ANOVA followed by Tukey-Kramer multiple comparison).

The distributions of bouton perimeters for each arbor type were skewed towards larger values (Fig. 6A). The histogram of normalized bouton counts in Figure 6A illustrates that the predominant peak perimeter of the cluster boutons was smaller than that of the diffuse and intermediate axonal boutons. Furthermore, the latter two distributions appeared to be quite similar. Cumulative probability plots indicated that the bouton perimeters associated with the cluster arborization were significantly different than those of the intermediate or diffuse types (Fig. 6A, inset; K-S test; $P < 0.01$). Although the cumulative probability plots of bouton perimeters for intermediate and diffuse populations appeared to be quite similar, they were also significantly different (K-S test; $P < 0.01$). From our initial microscopic observations, it appeared that the boutons in the cluster were predominantly small and somewhat uniform in appearance, whereas those in the intermediate and diffuse arborizations were variable in size, with both small and larger sized boutons. To further evaluate this observation, we fitted multiple Gaussian distributions to best approximate the total population of bouton perimeters. The distributions of bouton perimeters for individual neurons and the total population for each type of arborization were all best fitted by the sum of two Gaussian distributions (Fig. 6B). For all three types of arborizations, the primary Gaussian distribution accounted for approximately 80% of the bouton population, whereas the secondary distribution encompassed the remaining 20% (Fig. 6B). Although each arbor type apparently contained two normally distributed subpopulations of boutons, the means of each subpopulation for the clusters (small, 3.0 μm; large, 4.8 μm) were smaller than the corresponding values for intermediate or (small, 4.0 μm; large, 6.2 μm) or diffuse (small, 3.8 μm; large, 5.6 μm) types. Intermediate and diffuse arborizations tended to have higher proportions of larger boutons. For example, the percentages of boutons with perimeters greater than 6 μm in the intermediate (14.6%) and the diffuse (12.8%) arborizations were more than double the percentage present within the cluster arborizations (5.3%).

Differences in the density of axonal swellings were revealed when similar sized microscopic fields of the different arborizations were compared (Fig. 4Aii,Bii,Cii). The density of axonal swellings was correlated with the type of arborization. The cluster arborization had the highest average density of swellings (20.6 ± 1.7 boutons/900 μm^2), those of the intermediate type were less dense (15.7 ± 0.8 boutons/900 μm^2), and those of diffuse arborizations had the lowest average density (8.7 ± 0.5 boutons/900 μm^2). The contour plots of bouton density in Figure 7A–C correspond to the camera lucida drawings in Figures 1A, 2, and 3, respectively, and clearly illustrate both the differences in bouton density and in area distribution for the three different arborizations. The cluster arborization contained a high density of boutons in a small core area (Fig. 7A). By contrast, the intermediate arborization encompassed a much larger area and had multiple regions of moderate bouton density (Fig. 7B); however, the peak bouton densities were only approximately 50% of the cluster (cf. Fig. 7A,B). The diffuse arborization (Fig. 7C) had a significantly lower overall bouton density without the centralized regions of higher density that characterized the intermediate and cluster arborizations.

Cytochrome-oxidase and PV reactivity

To gain perspective on the relationship of nRt projection patterns in VB to features of the intrinsic anatomical organization of the nucleus, we examined the "barreloids" located within VPM known to be receptive areas for sensory input from single vibrissae on the snout (Van der Loos, 1976; Land and Simons, 1985). We hypothesized that the tightly clustered type of nRt axonal termination might relate spatially to these somatotopic structures. Two approaches were used to stain the barreloids. Cytochrome-oxidase staining in rodents is known to reveal the barreloids as patchy regions of increased metabolic activity in VPM (Van der Loos, 1976; Land and Simons, 1985). The visibility of this barreloid pattern has been shown to be heavily dependent on the plane of section (Land and Simons, 1985). When we obtained cytochrome oxidase-stained sections, we observed a clearly defined pattern within VPM similar to what has been previously described (Fig. 8A).

A second approach to defining the barreloids involved staining with an antibody to PV. Virtually all neurons within nRt contain GABA and are PV immunoreactive (Houser et al., 1980; Seto-Ohsima et al., 1989; Celio, 1990). Results of PV staining in a horizontal thalamic slice are shown in Figure 8. We found that the majority of somata in nRt were PV immunoreactive (Fig. 8B). By contrast, no somata in VB were PV immunoreactive; however, PV^+ fibers traveling in the presumed path of nRt-VB projections were obvious in VB at higher magnifications (not shown). Furthermore, in the same horizontal sections, the PV^+ fibers in VPM formed a barreloid-like pattern that was similar to that revealed with cytochrome-oxidase staining (cf. Fig. 8A,B). With higher magnification, individual barreloids were quite obvious (Fig. 8Ci). When single cluster arborizations of nRt neurons were superimposed on representative barreloids, it became obvious that the size and shape of the cluster arborizations roughly approximated those of individual barreloids (Fig. 8Cii). The relatively high density of boutons found in the cluster arborizations may contribute to the nonuniform PV^+ fiber staining observed within VPM. It also appeared that the various orientations of the cluster axonal arborizations were remarkably consistent with the multiple orientations of the barreloids in horizontal sections (see, e.g., Fig. 8Cii).

Electrophysiological properties of nRt neurons with different axonal arbors

The average resting potential for all labelled neurons was −61.0 ± 1.1 mV (n = 37) and did not differ significantly between axon types (Table 2). By contrast, the R_N of neurons with diffuse arborizations averaged 182.9 ± 15.1 MΩ, which was significantly higher than that for cells associated with either the cluster (139.6 ± 13.7 MΩ) or the

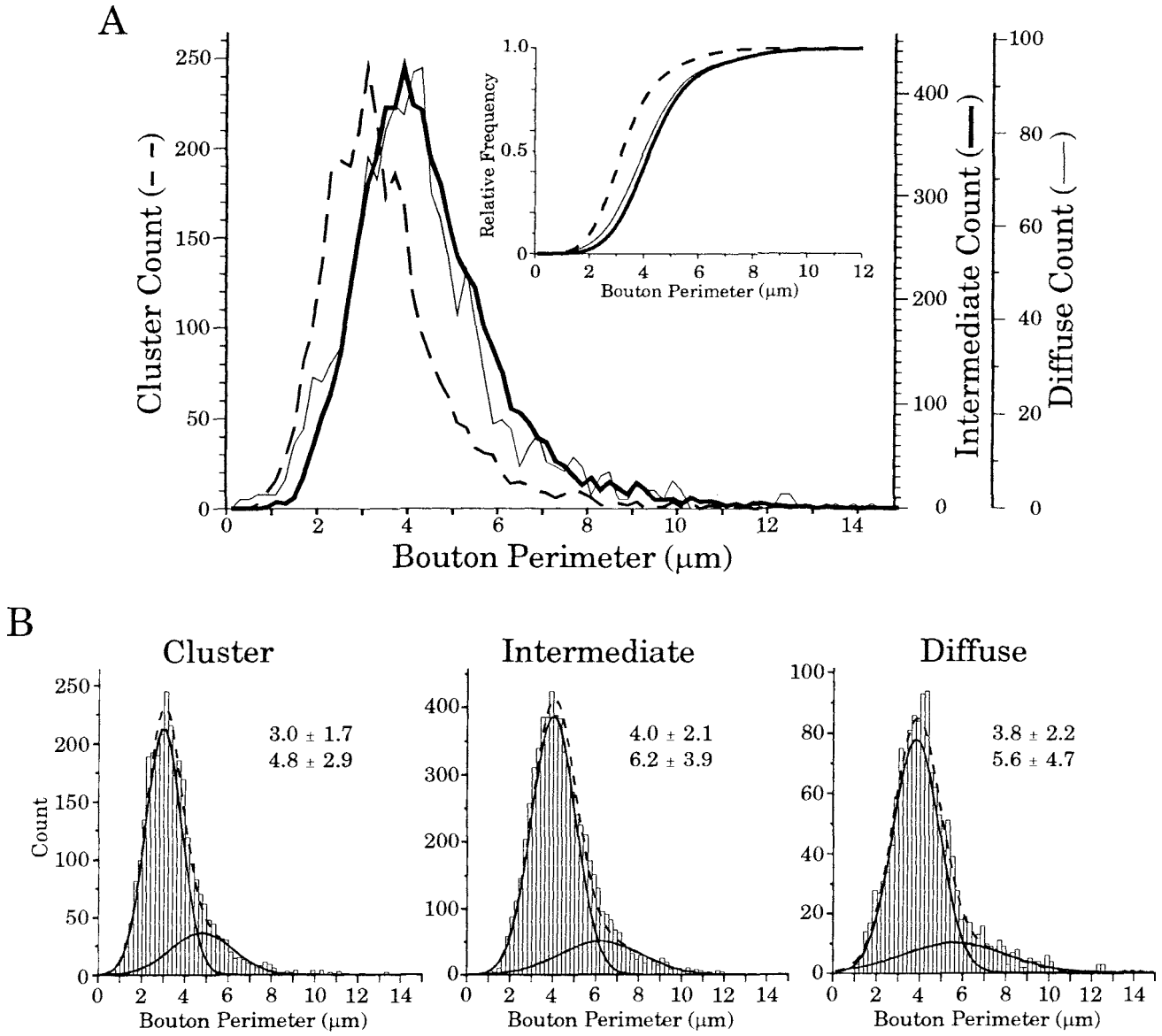

Fig. 6. Distribution of bouton perimeters for each arborization type. **A:** Standardized histograms (bin width, 0.2 μm) of bouton perimeters for the cluster (dashed line; n = 2,968), intermediate (thick line; n = 6,400), and diffuse arborizations (thin line: n = 1,394). **Inset:** Cumulative probability plots for each of the corresponding distributions in A. **B:** Histograms showing the distribution for each axon type. The solid lines are the two Gaussian distributions used to fit the raw data. Numbers indicate the mean and standard deviation for each. The dashed line is the sum of the two Gaussian subpopulations.

intermediate arborizations (136.1 ± 10.8 MΩ; $P < 0.05$). Neurons with diffuse arborizations had a slower membrane time constant than that of intermediate or cluster neurons; however, this difference was not statistically significant. Comparisons of spike amplitude, threshold, width, rate of rise, and rate of decay (Table 2) revealed no significant differences among neurons within the three classes of axonal arbors.

DISCUSSION

The thalamic reticular nucleus serves as a major inhibitory input to thalamic relay nuclei. Thus, the projection of nRt neurons upon relay neurons will have profound influences on thalamocortical activity. This study provides clear evidence that the anatomic projections of nRt neurons within thalamic relay nuclei are heterogeneous. Individual nRt neurons can give rise to one of three axonal arborizations: cluster, intermediate, or diffuse. These arborization patterns are present throughout VB and are not limited to a specific subdivision of VB. The presence of cluster arborizations provides a clear demonstration that nRt neurons can have very focal projections within dorsal thalamic nuclei. In VB, these arborizations are characterized by their compact area, the complexity of axonal ramifications, and the relatively high density of small axonal swellings. Each cluster arborization has a two-dimensional area that overlaps with approximately 50% of the dendritic area of a single VB neuron, indicating little divergence of this projection (certainly far less than that for diffuse or intermediate arbors). The intermediate specialization covers a larger area of VB and contains one or more regions of high bouton density.

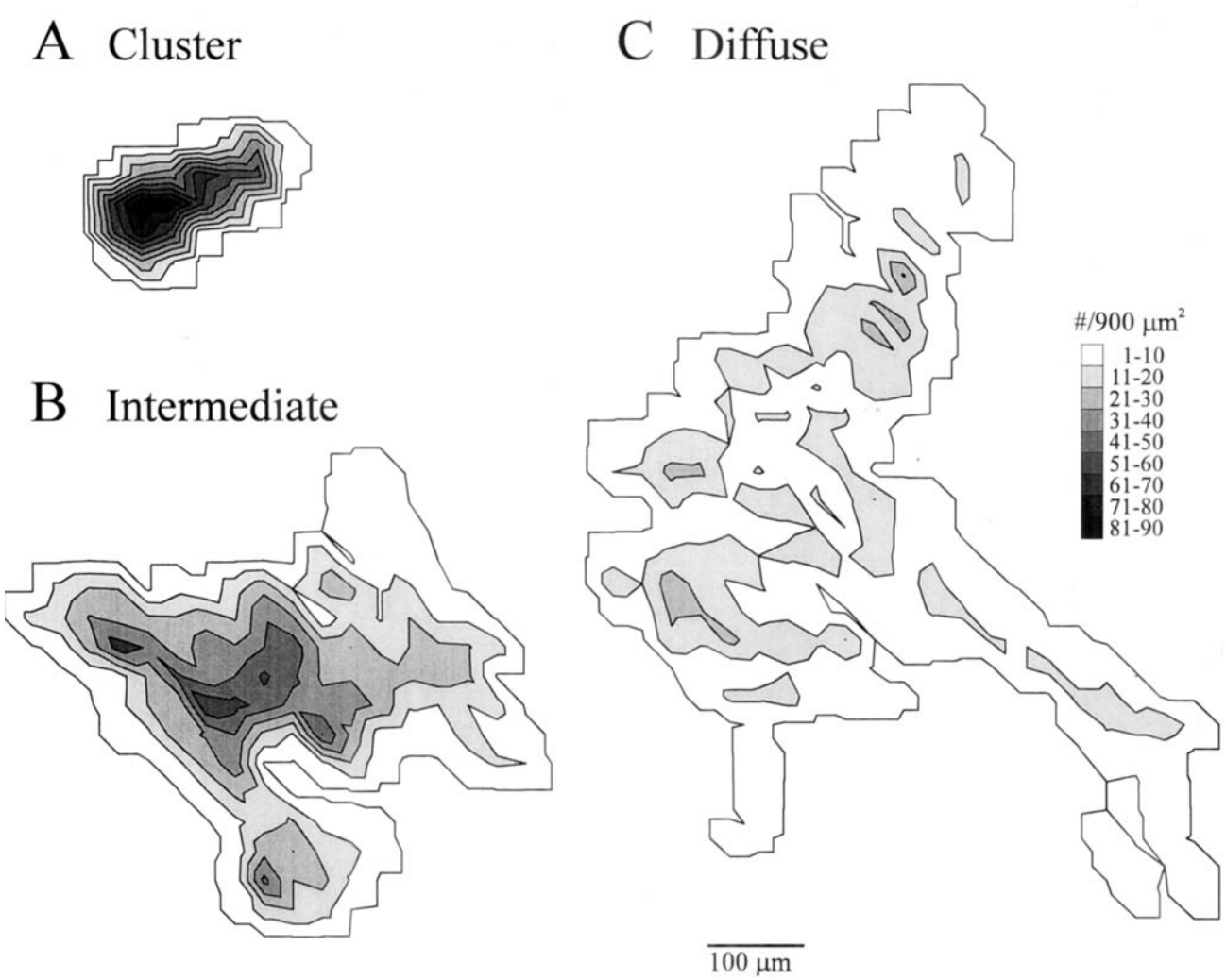

Fig. 7. Contour plots illustrating bouton density throughout the axonal arborization for the three different types of structures. Bouton density was quantified using a 30 × 30 μm grid. The plots of cluster, intermediate, and diffuse bouton density represent the cells illustrated in Figures 1A, 2, and 3, respectively.

The diffuse specialization consists of more divergent axonal branching and a relatively uniform bouton density across the entire arborization.

Elegant Golgi studies by Scheibel and Scheibel (1966) have revealed that single nRt neurons could innervate multiple thalamic nuclei in rodents. The axonal branching pattern in the dorsal thalamus was described as divergent and simple, suggesting that an individual nRt axon could project to a relatively large portion of the nucleus and could potentially make contact with a large number of neurons. Yen et al. (1985) examined the projections of individual physiologically identified somatosensory nRt neurons in VB by using intracellular injections of HRP. Their data indicated that nRt neurons in cats could project to multiple thalamic nuclei and that the axonal ramifications of single nRt neurons in VB were diffuse and encompassed a relatively large area of the nucleus, further supporting the general hypothesis of a diffuse projection of nRt neurons within thalamic relay nuclei. Our findings also support the presence of a diffuse projection in VB, but only in one-third of labelled rat nRt neurons. The remaining two-thirds of the nRt neurons have more localized projections that were not described in these earlier studies, suggesting multiple types of nRt projections in relay thalamus.

Other studies have suggested a more precise topographical relationship between nRt and dorsal thalamus (Montero et al., 1977; Hale et al., 1982; Crabtree and Killackey, 1989; Liu et al., 1995). The cluster arborization, with its clear focal projection, could serve as the anatomical substrate for a topographic relation between nRt and dorsal thalamus. The confined size and complexity of the cluster is strikingly similar to the lemniscal inputs in VB (see, e.g., Yen and Jones, 1983). Because we have labelled the connecting soma and made physiological recordings that are consistent with somatic electrode sites, our data clearly indicate that the cluster arborizations originate from nRt neurons. Results of a recent study using extracellular biocytin to label individual rat nRt neurons suggest that all projections within VB from nRt are focal (Pinault et al., 1995a). Our results differ, in that we observed these focal cluster arborizations in only about one-third of the labelled neurons. The different results obtained in the experiments of Yen et al. (1985), Pinault et al. (1995a), and the present study may be a consequence of the different labelling

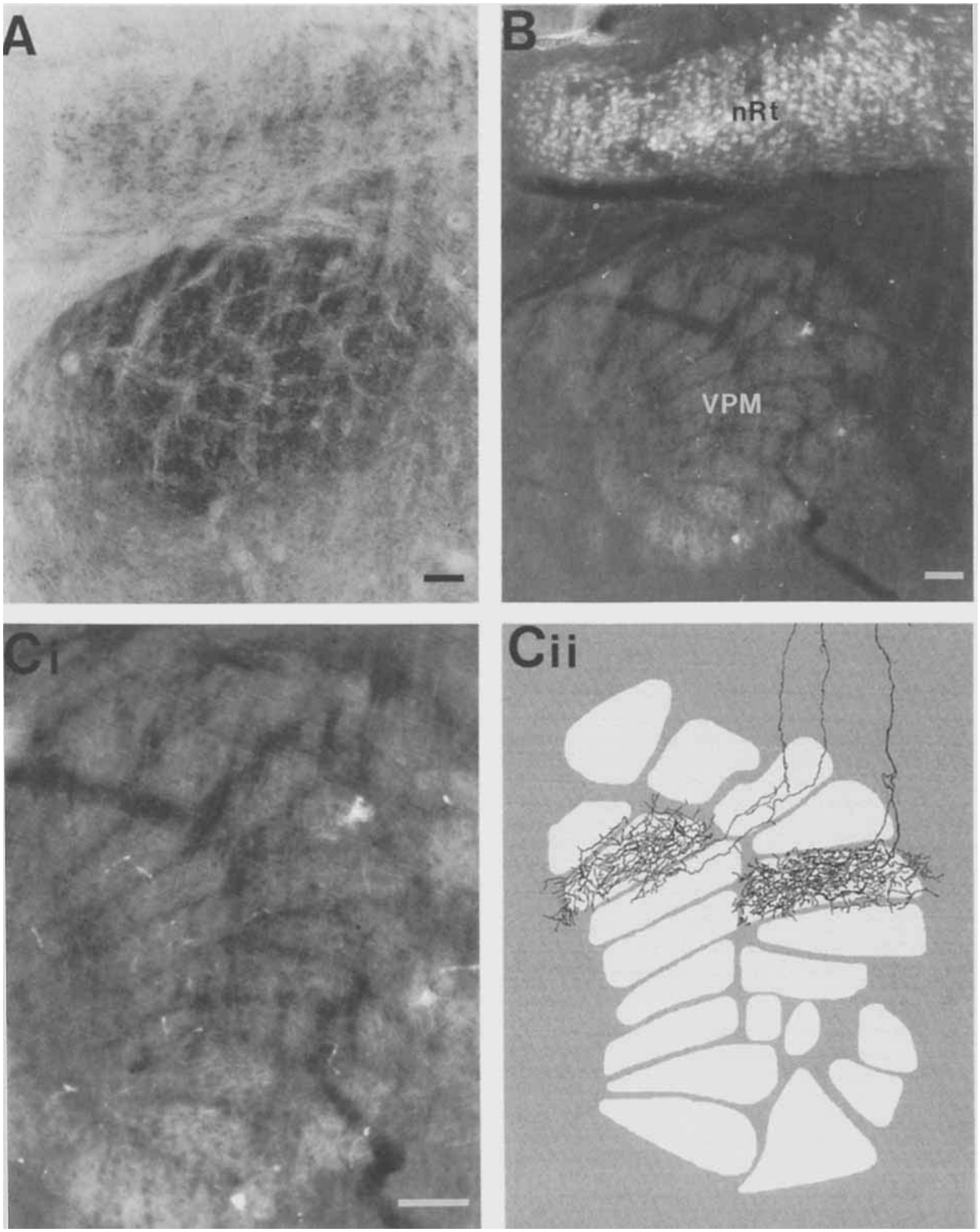

Fig. 8. **A:** Low-power photomicrograph of cytochrome-oxidase staining in a horizontal thalamic section. Note that nRt and ventroposteromedial nuclei (VPM) have been labelled in B. **B:** Photomicrograph of parvalbumin immunoreactivity conjugated to the fluorescent marker Texas red within a horizontal thalamic section similar to that in A. Note the bright staining of the nRt neurons in the top portion of the micrograph. Within VPM, the parvalbumin immunoreactivity is discontinuous and forms a barreloid-like pattern similar to that in A. **Ci:** A higher magnification of the VPM shown in B clearly illustrates the barreloid pattern. **Cii:** Two different cluster arborizations are superimposed on a schematic of the barreloid pattern from Ci. The scale of the schematic is equivalent to that in Ci. The somata associated with these clusters have been properly oriented within nRt, thus indicating various orientations of arborizations in VB (see Fig. 1, insets). The schematic and cluster arborizations are at equivalent scales. Scale bars = 100 μm.

TABLE 2. Physiological Characteristics of nRt Neurons With Different Axonal Arborization[1]

Arborization	V_m (mV)	R_N (MΩ)	τ_m (msec)	Spike amplitude (mV)	Spike threshold (mV)	Spike width (msec)	dV/dt rise (mV/msec)	dV/dt fall (mV/msec)
Cluster	−60.2 ± 2.2 (11)	138.7 ± 13.7 (11)	24.7 ± 2.7 (11)	79.2 ± 4.1 (9)	24.3 ± 1.6 (8)	0.70 ± 0.08 (8)	292.6 ± 35.4 (8)	−132.0 ± 27.5 (8)
Intermediate	−60.6 ± 2.0 (11)	133.2 ± 9.0 (11)	28.3 ± 3.2 (11)	80.7 ± 3.3 (11)	23.4 ± 1.9 (10)	0.70 ± 0.06 (11)	287.2 ± 31.8 (11)	−124.6 ± 10.4 (11)
Diffuse	−62.2 ± 1.6 (15)	189.7 ± 13.1 (14)*	30.0 ± 3.0 (14)	81.4 ± 2.1 (10)	23.9 ± 1.6 (10)	0.68 ± 0.04 (10)	317.5 ± 19.4 (10)	−120.2 ± 10.9 (10)

[1] V_m, resting membrane potential; R_N, input resistance; τ_m, membrane time constant; spike width, width measured at 50% spike amplitude; dV/dt Rise, rate of rise from 10–90% of spike amplitude; dV dt Fall, rate of decay from 90 to 10% of spike amplitude.
*$P < 0.01$ and 0.05 between diffuse and both intermediate and cluster, respectively (one-way ANOVA followed by Tukey-Kramer multiple comparison).

techniques and/or the intracellular tracers used. Alternatively, these dissimilar results may be due to a developmental process. Because diffuse and cluster axonal arborizations have been observed in young rodents (Scheibel and Scheibel, 1966; present study) and because only cluster-like arborizations have been observed in adult rodents (Pinault et al., 1995a), the diffuse arborizations may be the immature predecessor of the cluster axonal arborizations. Although this hypothesis remains to be tested directly in rodents, intracellular injections of individual nRt neurons have revealed the presence of diffuse axonal arborizations in adult cats (Yen et al., 1985).

Some investigators have hypothesized that nRt neurons can be categorized into different types based on soma shape and dendritic morphology (Spreafico et al., 1988, 1991). We have attempted to determine whether different axonal arborization types may be associated with different soma shape and size. Eighty-five percent of neurons with diffuse axonal arborizations had fusiform-shaped somata. On the other hand, both cluster and intermediate axonal arborizations were equally associated with either fusiform or round soma shapes. In addition, somata associated with the diffuse arborization were significantly smaller than those with the intermediate or cluster specializations. Spreafico et al. (1991) suggest that there are three populations of neurons within nRt, consisting of large fusiform (F), round (R), and small fusiform (f), that are distinguishable not only by general somatic morphology and location but also by dendritic orientation. Lubke (1993) also reported multiple shapes and sizes of nRt neurons but could not distinguish among the different soma types based on cell localization and dendritic orientation. On the basis of the size and shape of somata, the cluster and intermediate arbors may belong to F and R types of neurons, whereas the f-type neurons may have diffuse arbors; however, apparent differences in dendritic orientation or locale within nRt were not apparent in our data.

An obvious distinguishing characteristic among the different axonal arborizations was bouton density. The cluster arborization had a relatively high bouton density, whereas the boutons of the intermediate specialization were less dense and encompassed an area two to four times larger than boutons of the cluster specialization. The boutons of the diffuse specialization were uniformly distributed and low in density. If the density of the axonal swellings is indicative of the concentration of possible release sites, then these findings would suggest a potentially strong inhibitory influence in VB by a single cluster. The use of electron microscopy to assess the density of synaptic connections of individual nRt neurons within VB will be necessary to address this issue.

A number of physiological characteristics were compared among the neurons associated with these different arborizations. If the subtypes of arborizations are derived from different populations of nRt neurons, then it would seem reasonable to suggest that these cells may have different physiological properties (Friedlander et al., 1981; Contreras et al., 1992; Huguenard and Prince, 1992). Differences might include the neurotransmitter/neuropeptide phenotype, fine details of their synapses in the dorsal thalamus, or the nature and density of postsynaptic receptors. We did examine a number of intrinsic membrane characteristics, including resting membrane potential, membrane time constant, and action potential parameters (Table 2); however, these did not differ significantly between the arborization types. The smaller "diffuse" cells, as might be expected, had a significantly higher input resistance than the intermediate or cluster types. Although this difference could be reflected in an increased responsiveness to afferent synaptic activity, preliminary observations of synaptic potentials in response to electrical stimulation of internal capsule have not revealed any obvious qualitative differences among the different axonal groups (Cox, Huguenard, and Prince, unpublished observations).

Functional role of multiple axonal arborizations

Thalamic neurons generate action potentials in "burst" and "single spike" firing modes. These discharge patterns vary with the level of behavioral arousal and can influence the passage of sensory information from the periphery through the thalamus to the cortex (Steriade and Llinás, 1988; Steriade et al., 1993). The firing mode and the transition between modes is due in part to voltage-dependent intrinsic properties of thalamic neurons (Deschênes et al., 1982; Jahnsen and Llinás, 1984; Coulter et al., 1989; Steriade et al., 1993; Huguenard and Prince, 1994a). The reciprocal synaptic connectivity between nRt and dorsal thalamus gives rise to an intrathalamic circuit that is capable of generating rhythmic oscillatory activities. When these thalamic neurons are in burst mode, the oscillatory activities are similar to sleep spindles and to the spike and wave activity that is characteristic of absence epilepsy (Steriade and Llinás, 1988; Steriade et al., 1993; von Krosigk et al., 1993; Huguenard and Prince, 1994a).

The potency of nRt GABAergic output, which hyperpolarizes relay neurons by activating both $GABA_A$ and $GABA_B$ receptors (Hirsch and Burnod, 1987; Crunelli et al., 1988; Huguenard and Prince, 1994a), is a critical factor in regulating the firing mode of relay neurons. In this context, the topography and density of VB innervation by the three different arborization types may have important functional implications. For example, relatively few nRt neurons of the cluster and/or intermediate arborization types, with their relatively high bouton density, may form the anatomical substrate that produces a sufficient hyperpolarization to induce bursts of spike discharge in VB neurons. Burst

discharge of a single GABAergic perigeniculate neuron can result in a late afferent burst of excitatory postsynaptic potentials recorded in the same neuron, presumably by eliciting the synchronous burst discharge of one or more lateral geniculate relay neurons (Bal and McCormick, 1994). A similar interaction might occur between cluster-type nRt neurons and those in VB. Furthermore, this type of reciprocal connectivity between nRt and TC neurons may form an oscillatory unit or "sector." Thus, the more focal projections (cluster and intermediate) could serve to generate and maintain the oscillatory rhythms within a sector. In contrast, the diffuse arborizations may serve to synchronize multiple oscillatory sectors. We hypothesize that neurons possessing the diffuse and, to a lessor extent, the intermediate types of arborization could promote the spread of the oscillatory activity across nuclei in the dorsal thalamus, which has been demonstrated for spindle activity in ferret LGN (Kim et al., 1994).

Another aspect of the intrathalamic oscillations that remains unclear is the role of intra-nRt connectivity. Pharmacological disruption of the intranuclear inhibitory synapses may affect the robustness and duration of the intrathalamic rhythmicity (Huguenard and Prince, 1994b). Dendrodendritic synapses identified in monkey and cat may have a role in intra-nRt communication (Deschênes et al., 1985; Ohara, 1988); however, no such synapses have been identified in rodent nRt (Ohara, 1988). We observed fine axonal collaterals in approximately 65% of our filled neurons, suggesting recurrent connectivity among nRt neurons (Yen et al., 1985; Mulle et al., 1986; Spreafico et al., 1988; Lubke, 1993). This is in contrast to other recent studies in rat that have suggested that such collaterals are not present (Pinault et al., 1995a,b), but, again, this difference may be due to labelling methods. The presence of a low-density intra-nRt connectivity is consistent with ultrastructural studies showing a small population of symmetric synapses containing flattened vesicles (Ohara, 1988); however, there are other known inhibitory inputs to nRt (Asanuma and Porter, 1990).

The different axonal arborizations of nRt neurons are also likely to play an important role in the topographical relationship between nRt and VB. Barreloids in rodent VPM, which are the analogous structure to neocortical barrel fields, are revealed typically by cytochrome-oxidase or methylene-blue staining (Fig. 7A; Van der Loos, 1976; Land and Simons, 1985). However, a discontinuous staining pattern is also formed by PV^+ fibers in VPM (Celio, 1990; Frassoni et al., 1991) that is comparable to the barreloid pattern (Fig. 7B,Ci). Two primary PV^+ sources of these fibers are nRt and medial lemniscus (Jones and Hendry, 1989; Seto-Ohsima et al., 1989; Celio, 1990). Ultrastructurally, both symmetrical and asymmetrical PV^+ synapses have been observed in guinea pig VPM, suggesting that both nRt and medial lemniscal (ascending excitatory) fibers could be involved in this segregated staining (De Biasi et al., 1994). Anti-GABA antibody staining also reveals barreloid-like patterns in VPM, further supporting the participation of nRt projections in the barreloid structures (Huguenard and Prince, 1992). Our results show that the compact size and shape of the cluster is strikingly similar to that of the barreloids (see Fig. 8). This pattern of connectivity suggests that there is a precise topographical relationship between nRt and VPM and that small groups of nRt neurons may have a strong inhibitory influence on single barreloids. Presumably, this topographic relationship between nRt and relay thalamus is not restricted to VPM, because cluster arborizations were also observed in VPL.

Stimulation of nRt, as might be predicted, can selectively regulate cortical evoked potentials generated via thalamic relay neurons (Yingling and Skinner, 1976). In single-unit recordings from VB, stimulation of surrounding whiskers can attenuate the excitatory response to subsequent stimulation of the primary "best response" whisker (Simons and Carvell, 1989). In contrast to the relatively strong surround inhibition observed within the cortical barrels, not all surrounding whiskers attenuated the response to the primary whisker in somatosensory thalamus, and the degree of inhibition was variable (Hellwig et al., 1977; Simons and Carvell, 1989). The different patterns of innervation by the cluster and intermediate arborizations could be the anatomical correlates that underlie the variability of the surround inhibition observed in VB. The role of nRt in the shaping of receptive fields is further supported by experiments in which the receptive fields of individual VPM neurons were enlarged following lesions of nRt (Lee et al., 1994). In addition, the magnitude of response was increased, which is indicative of a feedback inhibition by nRt. The focal projection of cluster arborizations could also serve to finely tune receptive fields, in this case, by influencing the neuronal activity within single adjacent barreloids; whereas the intermediate arbor could influence multiple barreloids. Furthermore, these focal projections are not limited to somatosensory thalamus. Similar projections have also been observed in the LGN (Uhlrich et al., 1991; Pinault et al., 1995b). The heterogeneity of innervation by nRt within dorsal thalamus suggests that nRt is not merely a broad diffuse inhibitory network, but, in fact, it has a potentially active and selective role in the regulation of thalamocortical activities.

ACKNOWLEDGMENTS

We thank I. Parada, P. Riquelmo, E. Brooks, and A. De Haas-Johnson for their excellent technical assistance and B. Bennett for helpful discussions. This work was supported by National Institutes of Health Grants NS06477 and NS07280 and by the Morris and Pimley Research Funds.

LITERATURE CITED

Ahlsén, G., S. Lindström, and F. Lo (1985) Interaction between inhibitory pathways to principal cells in the lateral geniculate nucleus of the cat. Exp. Brain Res. *58*:134–143.

Asanuma, C., and L.L. Porter (1990) Light and electron microscopic evidence for a GABAergic projection from the caudal basal forebrain to the thalamic reticular nucleus in rats. J. Comp. Neurol. *302*:159–172.

Bal, T., and D.A. McCormick (1994) PGN and relay neurons form reciprocal monosynaptic connections in the LGNd. Soc. Neurosci. Abstr. *20*:8.

Blanton, M.G., J.J. Lo Turco, and A.R. Kriegstein (1989) Whole cell recording from neurons in slices of reptilian and mammalian cerebral cortex. J. Neurosci. Methods *30*:203–210.

Celio, M.R. (1990) Calbindin D28k and parvalbumin in rat nervous system. Neuroscience *35*:375–475.

Conley, M., and I.T. Diamond (1990) Organization of the visual sector of the thalamic reticular nucleus in galago. Eur. J. Neurosci. *2*:211–226.

Contreras, D., R. Curró Dossi, and M. Steriade (1992) Bursting and tonic discharges in two classes of reticular thalamic neurons. J. Neurophysiol. *68*:973–977.

Coulter, D.A., J.R. Huguenard, and D.A. Prince (1989) Calcium currents in rat thalamocortical relay neurones: Kinetic properties of the transient, low-threshold current. J. Physiol. (London) *414*:587–604.

Cox, C.L., J.R. Huguenard, and D.A. Prince (1994) Cholecystokinin (CCK) depolarizes neurons of thalamic reticular nucleus (nRt) and reduces intrathalamic rhythmicity (abstract). Epilepsia *35:*63.

Crabtree, J.W. (1992) The somatotopic organization within the rabbit's thalamic reticular nucleus. Eur. J. Neurosci. *4:*1343–1351.

Crabtree, J.W., and H.P. Killackey (1989) The topographic organization and axis of projection within the visual sector of the rabbit's thalamic reticular nucleus. Eur. J. Neurosci. *1:*94–109.

Crunelli, V., M. Haby, D. Jassik-Gerschenfeld, N. Leresche, and M. Pirchio (1988) Cl^- and K^+-dependent inhibitory postsynaptic potentials evoked by interneurones of the rat lateral geniculate nucleus. J. Physiol. (London) *399:*153–176.

De Biasi, S., P. Arcelli, and R. Spreafico (1994) Parvalbumin immunoreactivity in the thalamus of the guinea pig: Light and electron microscopic correlation with gamma-aminobutyric acid immunoreactivity. J. Comp. Neurol. *348:*556–569.

Deschênes, M., J.P. Roy, and M. Steriade (1982) Thalamic bursting mechanism: An inward slow current revealed by membrane hyperpolarization. Brain Res. *239:*289–293.

Deschênes, M., A. Madariaga-Domich, and M. Steriade (1985) Dendrodendritic synapses in the cat reticularis thalami nucleus: A structural basis for thalamic spindle synchronization. Brain Res. *334:*165–168.

Domich, L., G. Oakson, and M. Steriade (1986) Thalamic burst patterns in the naturally sleeping cat: A comparison between cortically-projecting and reticularis neurones. J. Physiol. (London) *379:*429–449.

Frassoni, C., M. Bentivoglio, R. Spreafico, M.P. Sanchez, L. Puelles, and A. Fairen (1991) Postnatal development of calbindin and parvalbumin immunoreactivity in the thalamus of the rat. Dev. Brain Res. *58:*243–249.

Friedlander, M.J., C.-S. Lin, L.R. Stanford, and S.M. Sherman (1981) Morphology of functionally identified neurons in lateral geniculate nucleus of the cat. J. Neurophysiol. *46:*80–129.

Hale, P.T., A.J. Sefton, L.A. Baur, and L.J. Cottee (1982) Interrelations of the rat's thalamic reticular and dorsal lateral geniculate nuclei. Exp. Brain Res. *45:*217–229.

Hellwig, F.-C., W. Schultz, and O.D. Creutzfeldt (1977) Extracellular and intracellular recordings from cat's cortical whisker projection area: Thalamocortical response transformation. J. Neurophysiol. *40:*463–479.

Hirsch, J.C., and J. Burnod (1987) A synaptically evoked late hyperpolarization in the rat dorsolateral geniculate neurons in vitro. Neuroscience *23:*457–468.

Horikawa, K., and W.E. Armstrong (1988) A versatile means of intracellular labeling: Injection of biocytin and its detection with avidin conjugates. J. Neurosci. Methods *25:*1–11.

Houser, C.R., J.E. Vaughn, R.P. Barber, and E. Roberts (1980) GABA neurons are the major cell type of the nucleus reticularis thalami. Brain Res. *200:*341–354.

Huguenard, J.R., and D.A. Prince (1992) A novel T-type current underlies prolonged Ca^{2+}-dependent burst firing in GABAergic neurons of rat thalamic reticular nucleus. J. Neurosci. *12:*3804–3817.

Huguenard, J.R., and D.A. Prince (1994a) Intrathalamic rhythmicity studies in vitro: Nominal t-current modulation causes robust antioscillatory effects. J. Neurosci. *14:*5485–5502.

Huguenard, J.R., and D.A. Prince (1994b) Clonazepam suppresses $GABA_B$-mediated inhibition in thalamic relay neurons through effects in nucleus reticularis. J. Neurophysiol. *71:*2576–2581.

Jahnsen, H., and R. Llinás (1984) Electrophysiological properties of guinea-pig thalamic neurones: An in vitro study. J. Physiol. (London) *349:*205–226.

Jones, E.G. (1975) Some aspects of the organization of the thalamic reticular complex. J. Comp. Neurol. *162:*285–308.

Jones, E.G. (1985) The Thalamus. New York: Plenum Press.

Jones, E.G., and S.H.C. Hendry (1989) Differential calcium binding protein immunoreactivity distinguishes classes of relay neurons in monkey thalamic nuclei. Eur. J. Neurosci. *1:*222–246.

Kim, U., T. Bal, and D.A. McCormick (1994) Spindle oscillations in the ferret LGNd are traveling waves. Soc. Neurosci. Abstr. *20:*133.

Land, P.W., and D.J. Simons (1985) Metabolic and structural correlates of the vibrissae representation in the thalamus of the adult rat. Neurosci. Lett. *60:*319–324.

Lee, S.M., M.H. Friedberg, and F.F. Ebner (1994) The role of GABA-mediated inhibition in the rat ventral posterior medial thalamus. I. Assessment of receptive field changes following thalamic reticular nucleus lesions. J. Neurophysiol. *71:*1702–1715.

Liu, X., R.A. Warren, and E.G. Jones (1995) Synaptic distribution of afferents from reticular nucleus in ventroposterior nucleus of cat thalamus. J. Comp. Neurol. *352:*187–202.

Lubke, J. (1993) Morphology of neurons in the thalamic reticular nucleus (TRN) of mammals as revealed by intracellular injections into fixed brains. J. Comp. Neurol. *329:*458–471.

Minderhoud, J.M. (1971) An anatomical study of the efferent connections of the thalamic reticular nucleus. Exp. Brain Res. *12:*435–446.

Montero, V.M., R.W. Guillery, and C.N. Woolsey (1977) Retinotopic organization within the thalamic reticular nucleus demonstrated by a double label autoradiographic technique. Brain Res. *138:*407–421.

Mulle, C., A. Madariaga, and M. Deschênes (1986) Morphology and electrophysiological properties of reticularis thalami neurons in cat: In vivo study of a thalamic pacemaker. J. Neurosci. *6:*2134–2145.

Ohara, P.T. (1988) Synaptic organization of the thalamic reticular nucleus. J. Electr. Microsc. Tech. *10:*283–292.

Ohara, P.T., and A.R. Lieberman (1981) Thalamic reticular nucleus: Anatomical evidence that cortico-reticular axons establish monosynaptic contact with reticulo-geniculate projection cells. Brain Res. *207:*153–156.

Ottersen, O.P., and J. Storm-Mathisen (1984) GABA-containing neurons in the thalamus and pretectum of the rodent. An immunocytochemical study. Anat. Embryol. *170:*197–207.

Paxinos, G., and C. Watson (1986) The Rat Brain in Stereotaxic Coordinates. Orlando, FL: Academic Press.

Pinault, D., J. Bourassa, and M. Deschênes (1995a) Thalamic reticular input to the rat visual thalamus: A single fiber study using biocytin as an anterograde tracer. Brain Res. *670:*147–152.

Pinault, D., J. Bourassa, and M. Deschênes (1995b) The axonal arborization of single thalamic reticular neurons in the somatosensory thalamus of the rat. Eur. J. Neurosci. *7:*31–40.

Press, W.H., B.P. Flannery, S.A. Teukolsky, and W.T. Vetterling (1986) Numerical Recipes. Cambridge: Cambridge University.

Scheibel, M.E., and A.B. Scheibel (1966) The organization of the nucleus reticularis thalami: A golgi study. Brain Res. *1:*43–62.

Seto-Ohsima, A., E. Aoki, R. Semba, P.C. Emson, and C.W. Heizmann (1989) Parvalbumin immunoreactivity in the reticular thalamic nucleus of developing rats. Acta Histochem. Cytochem. *22:*331–340.

Shosaku, A., Y. Kayama, I. Sumitomo, M. Sugitani, and K. Iwama (1989) Analysis of recurrent inhibitory circuit in rat thalamus: Neurophysiology of the thalamic reticular nucleus. Progr. Neurobiol. *32:*77–102.

Simons, D.J., and G.E. Carvell (1989) Thalamocortical response transformation in the rat vibrissa/barrel system. J. Neurophysiol. *61:*311–330.

Spreafico, R., M. DeCurtis, C. Frassoni, and G. Avanzini (1988) Electrophysiological characteristics of morphologically identified reticular thalamic neurons from rat slices. Neuroscience *27:*629–638.

Spreafico, R., G. Battaglia, and C. Frassoni (1991) The reticular thalamic nucleus (RTN) of the rat: Cytoarchitectural, golgi, immunocytochemical, and horseradish peroxidase study. J. Comp. Neurol. *304:*478–490.

Steriade, M., and R. Llinás (1988) The functional states of the thalamus and the associated neuronal interplay. Physiol. Rev. *68:*649–742.

Steriade, M., D.A. McCormick, and T.J. Sejnowski (1993) Thalamocortical oscillations in the sleeping and aroused brain. Science *262:*679–685.

Tseng, G., I. Parada, and D.A. Prince (1991) Double-labelling with rhodamine beads and biocytin: A technique for studying corticospinal and other projection neurons in vitro. J. Neurosci. Methods *37:*121–131.

Uhlrich, D.J., J.B. Cucchiaro, A.L. Humphrey, and S.M. Sherman (1991) Morphology and axonal projection patterns of individual neurons in the cat perigeniculate nucleus. J. Neurophysiol. *65:*1528–1541.

Van der Loos, H. (1976) Barreloids in mouse somatosensory thalamus. Neurosci. Lett. *2:*1–6.

von Krosigk, M., T. Bal, and D.A. McCormick (1993) Cellular mechanisms of a synchronized oscillation in the thalamus. Science *261:*361–364.

Williams, D. (1953) A study of thalamic and cortical rhythms in petit mal. Brain *76:*50–69.

Wong-Riley, M. (1979) Changes in the visual system of monocularly sutured or enucleated cats demonstrable with cytochrome oxidase histochemistry. Brain Res. *171:*11–28.

Yen, C.T., and E.G. Jones (1983) Intracellular staining of physiologically identified neurons and axons in the somatosensory thalamus of the cat. Brain Res. *280:*148–154.

Yen, C.T., M. Conley, S.H.C. Hendry, and E.G. Jones (1985) The morphology of physiologically identified GABAergic neurons in the somatic sensory part of the thalamic reticular nucleus in the cat. J. Neurosci. *5:*2254–2268.

Yingling, C.D., and J.E. Skinner (1976) Selective regulation of thalamic sensory relay nuclei by nucleus reticularis thalami. Electroencephalogr. Clin. Neurophysiol. *41:*476–482.